Effect of Extended Fringing Fields on Ion-Focusing Properties of Deflecting Magnets

Cite as: Review of Scientific Instruments **35**, 278 (1964); https://doi.org/10.1063/1.1718806
Submitted: 29 August 1963 . Published Online: 29 December 2004

Harald A. Enge

holder. The boat holder is then retracted into the quartz tube, the boat storage rack (P) is moved into position, and the boat is lowered onto it. A worm gear moves the boat storage holder into position.

The aluminum boat storage chamber contains a window for observation and a leakproof door. The chamber is purged with inert gas. The handle shafts of the drive mechanisms proturding through the box are sealed with O-rings.

To test the uniformity of ingots cast in this apparatus, radioactive tracers were added to the original melt and their distribution measured in the cast ingots. As illustrated in Table I, the ingots were homogeneous and uniform. Experimental error in counting the tracers was $\pm 15\%$, and most samples from the ingots came within this range. Ingots containing radioactive indium and zinc seemed to be uniform, but there was some segregation of radioactive silver. However, the segregation of silver was minor when it is considered that the segregation coefficient of silver in InSb is about 10^{-5}. Autoradiographs of slices cut from these ingots showed no segregation of indium either at grain boundaries or at the surface. Zinc segregated in aggregates even for single crystal material. Silver segregated readily at the grain boundaries and in the last portions; however, the over-all distribution was uniform to freeze. Impurities other than zinc and silver are, of course, present in the InSb ingots, but these two were selected as typical impurities having a wide range in segregation coefficients.

As shown in Table II, ingots cast from the same batch of material gave similar amounts of n type material of almost like purity as indicated. The zone refining conditions were as nearly identical as possible. However, it was difficult to keep all conditions the same, such as the number of zone passes in the same single crystal state. Ingots from different bulk compoundings exhibited similar purity.

It is believed that this apparatus can be used for casting homogeneous ingots of metals, alloys, and semiconductor materials.

THE REVIEW OF SCIENTIFIC INSTRUMENTS VOLUME 35, NUMBER 3 MARCH 1964

Effect of Extended Fringing Fields on Ion-Focusing Properties of Deflecting Magnets

HARALD A. ENGE
Physics Department, Massachusetts Institute of Technology, Cambridge 39, Massachusetts

(Received 29 August 1963)

This paper presents the result of calculations on ion deflection and focusing in magnets that have realistic, extended fringing fields rather than sharply cutoff fringing fields. The most important effects of the change from sharp cutoff to extended fringing fields are (a) displacements of the beam center line at entrance and exit (a "zeroth-order" effect), and (b) reduction of first-order z-direction ("vertical") focusing. When the pole boundaries are curved or an effective curvature is caused by the proximity of pole-piece corners, there are further first-order effects on the trajectories. These effects can be minimized, and in practice made negligible, by correct centering of the beam relative to the pole-piece corners at entrance and exit.

I. INTRODUCTION

IN calculating the focusing properties of a homogeneous field magnet, it is customary to assume that the effects of the fringing field zones, which the particles are traveling through at the entrance and exit of the magnet, can be accounted for approximately by assuming that the magnetic induction is constant out to a "virtual field boundary" located at a distance from the pole edges of approximately $\frac{1}{2}$ to 1 air gap. We shall in the following refer to these types of calculations as calculations with a sharp cutoff fringing field (SCOFF). A recent paper by S. Penner[1] gives an excellent review on the subject of SCOFF calculations on homogeneous field magnets and magnetic quadrupole lenses. Investigations of the effect of an extended fringing field (EFF) on median-plane focusing have been undertaken by, for instance, Reutersward[2] and by Coggeshall.[3] The analyses in this paper are similar to those of Reutersward, except that a more realistic shape of the fringing-field curve is used, and focusing in the direction normal to the median plane of the magnet is also considered.

The aim of this paper is to present a unified treatment of the perturbations caused by an extended fringing field (EFF) as compared with a sharp cutoff fringing field (SCOFF). The assumption is made that, in the two cases, SCOFF and EFF, the particle trajectories coincide inside the magnet. The principal object of our investigation is then to study the differences between the SCOFF and EFF cases in trajectory location and direction outside the magnet, both on the entrance side and on the exit side.

[1] S. Penner, Rev. Sci. Instr. 32, 150 (1961).

[2] C. Reutersward, Arkiv Fysik 3, 53 (1952).

[3] N. D. Coggeshall, J. Appl. Phys. 18, 855 (1947).

Figure 1 shows the outline of the pole-piece area in a homogeneous field magnet with the virtual field boundaries indicated at the entrance and exit. It is assumed that the magnet is mirror symmetric around the median plane which is located in the center of the gap. A ray, defined as a central ray and marked SCOFF in Fig. 1, is a circle segment inside the virtual field boundaries and straight lines, tangents to the circle, outside these boundaries. The SCOFF orbit defines the x axes of an entrance coordinate system (x_0,y_0,z_0) and an exit coordinate system (x,y,z), both right-handed. Changes in the velocity components in the z direction are referred to as z-direction focusing, and changes in velocity components in the y direction, relative to the central ray, are referred to as median-plane focusing.

The position and slope of a particular trajectory at the exit $(x=0)$ can in general be expressed as power expansions in terms of the coordinates of positions and their derivatives (slopes) at the entrance $(x_0=0)$ and in terms of the relative change in momentum $\delta=\Delta p/p$ from that of the central ray. We introduce $y'=dy/dx$ and $z'=dz/dx$, etc., and write the result of SCOFF calculations in the following form:

$$\frac{y}{R}=(y/y)\frac{y_0}{R}+(y/y')y_0'+(y/\delta)\delta+(y/y^2)\left(\frac{y_0}{R}\right)^2$$
$$+(y/yy')\frac{y_0}{R}y_0'+(y/y\delta)\frac{y_0}{R}\delta+(y/y'^2)y_0'^2$$
$$+(y/y'\delta)y_0'\delta+(y/\delta^2)\delta^2+(y/z^2)\left(\frac{z_0}{R}\right)^2$$
$$+(y/zz')\frac{z_0}{R}z_0'+(y/z'^2)z_0'^2, \quad (1)$$

$$y'=(y'/y)\frac{y_0}{R}+(y'/y')y_0'+(y'/\delta)\delta+(y'/y^2)\left(\frac{y_0}{R}\right)^2$$
$$+(y'/yy')\frac{y_0}{R}y_0'+(y'/y\delta)\left(\frac{y_0}{R}\right)\delta+(y'/y'^2)y_0'^2$$
$$+(y'/y'\delta)y_0'\delta+(y'/\delta^2)\delta^2+(y'/z^2)\left(\frac{z_0}{R}\right)^2$$
$$+(y'/zz')\frac{z_0}{R}z_0'+(y'/z'^2)z_0'^2, \quad (2)$$

$$\frac{z}{R}=(z/z)\frac{z_0}{R}+(z/z')z_0'+(z/yz)\frac{y_0}{R}\frac{z_0}{R}$$
$$+(z/y'z)y_0'\frac{z_0}{R}+(z/\delta z)\delta\frac{z_0}{R}+(z/yz')\frac{y_0}{R}z_0'$$
$$+(z/y'z')y_0'z_0'+(z/\delta z')\delta z_0', \quad (3)$$

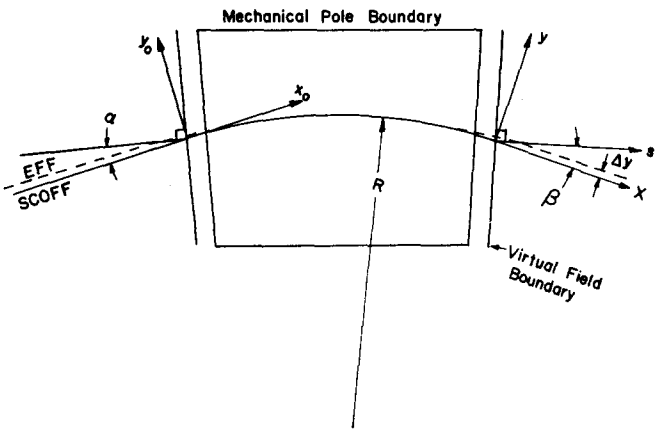

FIG. 1. Particle trajectories in sharp cutoff fringing field (SCOFF) and extended fringing field (EFF). Also shown are the entrance angle α, the exit angle β, and the coordinate systems used in the analytic calculations.

$$z'=(z'/z)\frac{z_0}{R}+(z'/z')z_0'+(z'/yz)\frac{y_0}{R}\frac{z_0}{R}$$
$$+(z'/y'z)y_0'\frac{z_0}{R}+(z'/\delta z)\delta\frac{z_0}{R}+(z'/yz')\frac{y_0}{R}z_0'$$
$$+(z'/y'z')y_0'z_0'+(z'/\delta z')\delta z_0'. \quad (4)$$

All third- and higher-order terms have been neglected, and the second-order terms that are zero because of the symmetry of the system have been left out. The displacements y and z have been made dimensionless by division by R, the radius of the central orbit. The coefficients of expansion are written in a form, e.g., (y'/yy'), which immediately identifies them.

If we look at Eqs. (1) to (4) as Taylor series, the coefficients are proportional to first- and second-order derivatives; for instance

$$(y'/y^2)=\frac{R^2}{2!}\frac{\partial^2 y'(y_0,y_0',z_0,z_0',\delta)}{\partial y_0^2}.$$

The coefficients are in general primarily functions of the parameters α, β, ϕ, R_a, R_b, R, W_a, W_b (Figs. 1 and 5), and the air gap D. For practical examples that have been studied, most coefficients have been found to be numerically of the order of magnitude of unity, only rarely is any coefficient larger than 2. It is quite clear, then, that if the beam characteristics are such that y_0/R, y', z_0/R, z_0', and δ are small compared to unity, all second-order terms in Eqs. (1) to (4) will be small compared with the first-order terms.

The first-order coefficients given by Penner[1] in matrix form[4] in the SCOFF approximation are listed in Table I.

A principal objective of this study is to determine how

[4] The same matrices, but without the δ term, were given in an earlier paper by M. Cotte, Ann. Phys. **10**, 333 (1938).

TABLE I. First-order transfer coefficients for a deflecting magnet.

$(y/y)=\dfrac{\cos(\phi-\alpha)}{\cos\alpha}$,	$(y/y')=\sin\phi$,	$(y/\delta)=1-\cos\phi$
$(y'/y)=-\dfrac{\sin(\phi-\alpha-\beta)}{\cos\alpha\cos\beta}$,	$(y'/y')=\dfrac{\cos(\phi-\beta)}{\cos\beta}$,	$(y'/\delta)=\sin\phi+(1-\cos\phi)\tan\beta$
$(z/z)=1-\phi\tan\alpha$,	$(z/z')=\phi$,	
$(z'/z)=-\tan\alpha-\tan\beta+\phi\tan\alpha\tan\beta$,	$(z'/z')=1-\phi\tan\beta$	

these first-order terms are changed when an extended fringing field is introduced. The second-order terms will be the subject of a forthcoming paper.

Another important point concerns the position of the central ray at the entrance and the exit. If we require that the beam in the EFF case coincides with the SCOFF center line inside the magnet, it will be displaced relative to it outside, both at the entrance and the exit (Fig. 1). This is because the field gradually decreases with distance from the magnet, and therefore the radius of curvature of the orbit increases gradually instead of, as in the SCOFF case, changing abruptly from R to infinity. The displacement, which is a zeroth-order effect (not depending upon y_0, y_0', etc.) is calculated in this work. The first-order coefficients given are redefined so that the variables y_0, y_0', y, and y' are measured from the EFF central ray rather than the SCOFF central ray.

It is relatively simple to show that in changing from a sharp cutoff fringing field to an extended fringing field, a reduction in over-all focusing strength results. The proof of this statement is given in the next section.

II. GENERAL PROOF OF FOCAL STRENGTH REDUCTION

From the theory of betatron oscillations in circular accelerators, we recall that small radial and z-direction (vertical) oscillations are governed by equations of the form[5]

$$d^2y/d\xi^2+[(1-n)/r^2]y=0,$$
$$d^2z/d\xi^2+(n/r^2)z=0. \tag{5}$$

Here, ξ is the curvilinear coordinate along the central ray, $r=r(\xi)$ is the radius of curvature of the central ray, y is the (small) displacement Δr from the central ray, and $n=n(\xi)$ is the field exponent defined as

$$n=-(r/B_z)dB_z/dr. \tag{6}$$

For any thin lens, optical or ion optical, the focal length f_y for motion in the $\xi-y$ plane can be defined through the equation

$$y/f_y=-\Delta(dy/d\xi), \tag{7}$$

[5] D. W. Kerst and R. Serber, Phys. Rev. **60**, 53 (1941).

and similarly for the z direction,

$$z/f_z=-\Delta(dz/d\xi). \tag{8}$$

The right-hand side of these equations represents a change in direction of a particle trajectory close to the central ray, compared with the direction of the central ray.

In a magnetic device, the change in slope $\Delta(dy/d\xi)$ is brought about by a difference in field and/or in length of the flight path between the central ray and another ray. The field gradient that causes the instantaneous change in $dy/d\xi$ is assumed to be a function of ξ. We can then generalize Eqs. (7) and (8) and write

$$\frac{1}{f_y}=-\int\frac{1}{y}\frac{d}{d\xi}\left(\frac{dy}{d\xi}\right)d\xi, \tag{7a}$$

and

$$\frac{1}{f_z}=-\int\frac{1}{z}\frac{d}{d\xi}\left(\frac{dz}{d\xi}\right)d\xi. \tag{8a}$$

The integrals, of course, are taken through the complete lens which is assumed to be thin. In particular, it is assumed that y or z does not change appreciably over the thickness of the lens.

For a lens with variable field gradient, the integrands in Eqs. (7a) and (8a) can be found from Eq. (5). By substitution, we find

$$1/f_y+1/f_z=\int d\xi/r^2. \tag{9}$$

Since the magnetic rigidity $B\rho$ of the particle is a constant of the motion, we can substitute $B_z r=B\rho$, and we then get

$$1/f_y+1/f_z=(B\rho)^{-2}\int B_z^2 d\xi. \tag{10}$$

The integral is taken through the lens along the central ray. It is emphasized again that the equation holds only for a thin lens; that is, a lens in which y and z do not change appreciably over the thickness of the lens. In particular, Eq. (10) does not at all give the correct focal strength of a

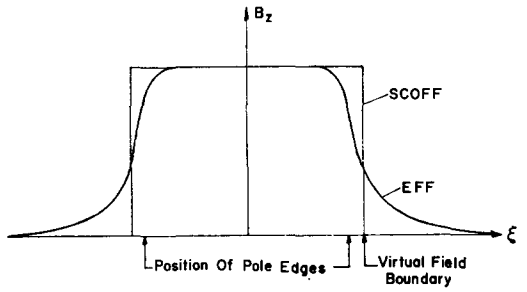

FIG. 2. These two field distributions give the same deflecting angle but different over-all focusing strengths.

quadrupole lens pair, which by no means represents a thin lens.

Consider a sector magnet, for which the angle of deflection is small and given by

$$\phi=(B\rho)^{-1}\int B_z d\xi. \tag{11}$$

Again the integral is taken along the central ray through the complete lens. In Fig. 2 are shown two field distributions that give rise to the same angle of deflection because the areas under the curves are the same [Eq. (11)]. Clearly, the integral of B_z^2 is not the same for the two distributions. It is larger for the rectangular distribution, and this therefore, according to Eq. (10), has the stronger focusing power. From this, it can be concluded that an extended fringing-field magnet is weaker focusing than the otherwise equivalent sharp cutoff fringing-field magnet. Equation (10) carries on the left-hand side the sum of the inverse focal lengths in the two directions, so that this introductory study does not reveal in which way the loss of focal strength is shared between the two directions. In the more detailed study below, it is shown that only the z-direction focal strength is reduced.

III. COMPARISON WITH SOLENOID AND QUADRUPOLE LENSES

It is interesting as an incidental point to compare Eq. (10) with the expression for the focal strength of an axial field lens[6] (solenoid lens, Glaser lens),

$$1/f=\tfrac{1}{4}(B\rho)^{-2}\int B_\xi^2 d\xi. \tag{12}$$

The integral is taken through the lens in the axial direction (ξ direction) which is also the field direction. In the sector magnet, which we might call a transverse-field lens, the entrance and exit angles can be adjusted so that the focal lengths are the same in the two planes ($f_y=f_z$). By comparing Eqs. (10) and (12), we then see that the transverse-field lens is just twice as strong as a longitudinal field lens with the same B vs ξ distribution. For further comparison, consider a quadrupole lens pair, in which the field strength at the pole tip is made numerically equal to the axial field in a solenoid lens. The over-all focusing power is then approximately a factor $2L^2/d^2$ stronger in the quadrupole pair than in the solenoid lens. L is the total length of the pair as well as of the solenoid, and d is the quadrupole aperture diameter. This formula shows that, for applications where L/d must be relatively small, nothing can be gained by using a quadrupole lens pair rather than a transverse field or axial field lens.

[6] See, for instance, L. Jacob, *An Introduction to Electron Optics* (Methuen and Company Ltd., London, 1951), p. 90.

IV. DETAILED ORBIT CALCULATIONS

Field Curves and Semiempirical Formulas for the Field

Figure 3 shows various observed fringing-field curves plotted against s', the distance from the pole edges in units of the air gap D. Sketches in true scale of the various coil and pole-piece configurations used for the field measurements are also shown in the figure. The measurements are carried out in the median plane normal to the pole-piece boundary and midway between the corners of the pole pieces. The ratio between the corner-to-corner distance W and the air gap D is given on the figure in each case.

An analytic expression that can be made to fit the experimental curves fairly well is

$$h(s)=B_{z,0}/B_0=1/(1+e^S), \tag{13}$$

where B_0 is the constant induction well inside the air gap and $B_{z,0}$ is the induction in the fringing field, as measured in the median plane ($z=0$). The parameter S is given by the power series

$$S=c_0+c_1 s+c_2 s^2+c_3 s^3. \tag{14}$$

Two functions calculated from Eqs. (13) and (14) are shown in Fig. 3. One is referred to as the short-tail curve obtained with the following values of the constants c,

$$c_0=0.3835,\quad c_1=2.388,\quad c_2=-0.8171,\quad c_3=0.200.$$

The other curve, the long-tail curve, is obtained with

$$c_0=0.531,\quad c_1=2.341,\quad c_2=-0.7799,\quad c_3=0.110.$$

The variable s in Eq. (14) is again the distance along the normal in units of D, but the origin for s has been placed at the "virtual field boundary"; that is, the integral under the actual field curve is equal to the integral of the sharp cutoff field curve starting at the origin. The pole edges are then approximately at $s=-0.62$ for the short-tail curve and $s=-0.68$ for the long-tail curve.

The general treatment below is not limited to fringing fields that can be expressed by Eq. (13). The numerical results quoted in the latter part of this report are, however,

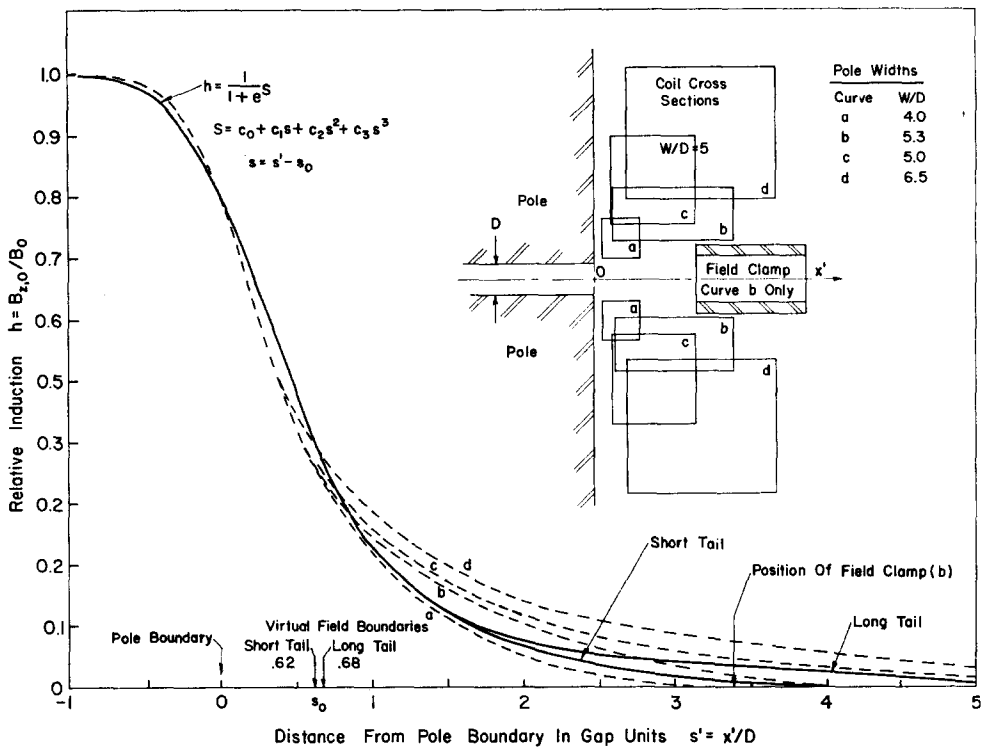

FIG. 3. Fringing-field curves calculated from Eq. (13) with two different sets of constants c (long-tail and short-tail). Curves measured for magnets with coil arrangements as indicated are shown for comparison.

based on such a description. Most of these results are based on calculations on the short-tail fringing field of Fig. 3, but some calculations have also been made on the long-tail fringing field.

We assume that the induction $B_{z,0}/B_0$ on the median plane of the magnet can be expressed by a function $h(s)$, which goes to zero for large positive values of s and to unity for large negative values of s. The assumption that h is a function of a linear coordinate s only implies that the pole-piece boundaries at entrance and exit are straight and that the effect of the proximity of the corners can be neglected. We assume further that the origin has been chosen so that

$$\int_{-s_1}^{\infty} h(s)ds = s_1, \tag{15}$$

provided $s_1 \gg 1$. This assures that the angle of deflection of particles going through this fringing field will be very nearly the same as for a sharp cutoff field terminating at the origin. Off the median plane, the z component has to be modified slightly, and there will also be an x and a y component. We use the general field equations to build up expressions for these components from the known induction on the median plane. The coordinates used are those shown in Fig. 1. The nondimensional coordinate s is given by

$$s = (x\cos\beta + y\sin\beta)/D. \tag{16}$$

Off the median plane the field components can be expressed in the form of a Taylor series in z, the distance from the median plane. Because of symmetry, the expression for B_z can only contain even powers of z, and the expressions for B_x and B_y can only contain odd powers of z. Neglecting terms higher than second order in z, we get for the z component

$$B_z = B_{z,0} + \frac{z^2}{2!}\left(\frac{\partial^2 B_z}{\partial z^2}\right)_{z=0}. \tag{17}$$

To determine the second-order derivative, we make use of Laplace's equation

$$\frac{\partial^2\phi}{\partial x^2} + \frac{\partial^2\phi}{\partial y^2} + \frac{\partial^2\phi}{\partial z^2} \equiv 0, \tag{18}$$

where ϕ is the scalar potential of the magnetic induction, and the identical sign means that the expression is equal to zero over all space in which we are interested. The derivative of Eq. (18) with respect to z must therefore also be equal to zero. This yields (with $B_z = -\partial\phi/\partial z$)

$$\frac{\partial^2 B_z}{\partial x^2} + \frac{\partial^2 B_z}{\partial y^2} + \frac{\partial^2 B_z}{\partial z^2} = 0, \tag{19}$$

which can be used to find the second-order derivative of B_z needed in Eq. (17). We substitute for B_z the value of the induction on the median plane $B_{z,0}$, which is a specified function of x and y expressed through the parameter s. Carrying through the substitution, we find the following second-order expression for the inductance in the z direction (valid also off the median plane):

$$B_z = B_0\left(h - \frac{z^2}{2D^2}\frac{d^2h}{ds^2}\right). \tag{20}$$

The first term in the Taylor expansion for the x component of the induction is

$$B_x=\frac{z}{1!}\left(\frac{\partial B_x}{\partial z}\right)_{z=0}=z\left(\frac{\partial B_{z,0}}{\partial x}\right)=\frac{z}{D}B_0\cos\beta\frac{dh}{ds}. \quad (21)$$

Here we have made use of the field equation curl $\mathbf{B}=0$. This expression is also good to second order in z, since the next nonzero term is in z^3. The corresponding expression for the induction in the y direction is

$$B_y=(z/D)B_0\sin\beta dh/ds. \quad (22)$$

Trajectories. Analytic Approach

The aim is to find the effect of the extended fringing field to first order in the quantities y/R, y', etc. It is not immediately clear whether terms that appear to be small to the second order may actually in the final analysis result in the corrections in first-order focusing that we are seeking. It seems therefore safest to carry initially all second-order terms. We can write Newton's second law for the motion of an ion with charge q and mass m through a magnetic field as

$$\frac{dv_x}{dt}=\frac{q}{m}(v_yB_z-v_zB_y), \quad (23)$$

$$\frac{d^2y}{dx^2}v_x^2+\frac{dy}{dx}\frac{dv_x}{dt}=\frac{q}{m}(v_zB_x-v_xB_z), \quad (24)$$

$$\frac{d^2z}{dx^2}v_x^2+\frac{dz}{dx}\frac{dv_x}{dt}=\frac{q}{m}(v_xB_y-v_yB_x). \quad (25)$$

Here we have treated y and z as functions of x, which again is a function of time t. Since the motion in the fringing field that we are considering is largely in the x direction, we can substitute

$$v\approx v_x(1+y'^2/2+z'^2/2). \quad (26)$$

We also make use of the expressions for the field components, Eqs. (20)–(22). With these substitutions and $qBR=mv$, the Eqs. (24) and (25) take the form

$$\frac{d^2y}{dx^2}=\frac{1}{R}\left[-h+\frac{z^2}{2D^2}\frac{d^2h}{ds^2}+\frac{dz}{dx}\frac{z}{D}\cos\beta\frac{dh}{ds}-\frac{3}{2}\left(\frac{dy}{dx}\right)^2h-\frac{1}{2}\left(\frac{dz}{dx}\right)^2h\right], \quad (27)$$

and

$$\frac{d^2z}{dx^2}=\frac{1}{R}\left[\frac{z}{D}\sin\beta\frac{dh}{ds}-\frac{dy}{dx}\frac{z}{D}\cos\beta\frac{dh}{ds}-\frac{dy}{dx}\frac{dz}{dx}h\right]. \quad (28)$$

We consider first motion in the median plane for which $z=0$ and $dz/dx=0$. Equation (27) then reduces to

$$\frac{d^2y}{dx^2}=-\frac{h}{R}\left[1+\frac{3}{2}\left(\frac{dy}{dx}\right)^2\right]. \quad (29)$$

This equation can be solved by successive approximations. The lowest-order term yields through integration from $-s_1$ to s

$$\frac{dy}{dx}-\left(\frac{dy}{dx}\right)_1=-\frac{D}{R\cos\beta}\int_{-s_1}^{s}hds, \quad (30)$$

where we have used

$$dx=(D/\cos\beta)ds. \quad (31)$$

Equation (30) inserted into (29) yields

$$\frac{d^2y}{dx^2}=-\frac{h}{R}\left\{1+\frac{3}{2}\left[\left(\frac{dy}{dx}\right)_1-\frac{D}{R\cos\beta}\int_{-s_1}^{s}hds\right]^2\right\}.$$

Integration of this equation gives

$$\frac{dy}{dx}-\left(\frac{dy}{dx}\right)_1=-\frac{D}{R\cos\beta}\int_{-s_1}^{s}hds+\frac{3D}{2R\cos\beta}\int_{-s_1}^{s}h\left[\left(\frac{dy}{dx}\right)_1-\frac{D}{R\cos\beta}\int_{-s_1}^{s}hds\right]^2ds. \quad (32)$$

We now introduce the SCOFF fringing-field function

$$\begin{aligned}h_0(s)&=1 \text{ for } x<0\\&=0 \text{ for } x\geq 0\end{aligned} \quad (33)$$

and attempt to find the difference in change of slope [Eq. (32)] between the EFF system with $h=h(s)$ and the SCOFF system with $h=h_0(s)$.

The center line of the SCOFF system at the exit defines the x axis. Therefore, dy/dx is zero for the SCOFF central ray outside the magnet. Inside, at point $-s_1$, it is approximately $s_1D/R\cos\beta$. With this inserted into the last term of Eq. (32), the integral can be evaluated. The difference in this integral, as determined for the SCOFF case and for the EFF case with any reasonable fringing-field function $h(s)$, is small compared to unity. For other rays close to the center line [rays with different $(dy/dx)_1$], the same statement applies. Since the term considered is of third order in D/R, we can safely neglect it in this work.

The first term of Eq. (32) yields with (15)

$$\left(\frac{dy}{dx}\right)=\left(\frac{dy}{dx}\right)_1-\frac{s_1D}{R\cos\beta}, \quad (34)$$

independent of the exact form of $h(s)$. We can therefore draw the important conclusion that *there is no resultant change in direction of a ray in the median plane in going from the SCOFF to the EFF case.*

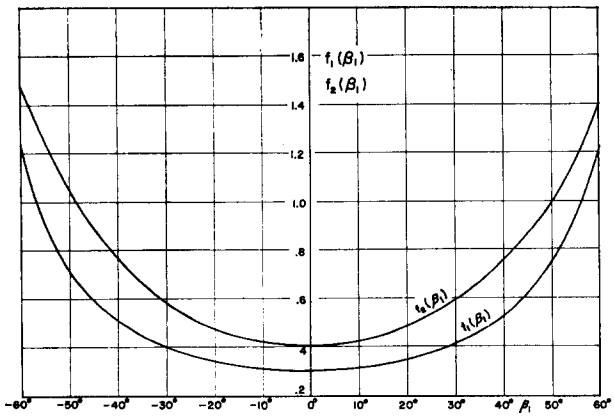

FIG. 4. Functions entering into Eq. (41) for the center line displacement and Eq. (42) for the reduction of z-directional focal strength (based on the short-tail fringing-field curve).

A second integration of Eq. (32), again neglecting the last term, yields

$$y-y_1=\left(\frac{dy}{dx}\right)_1(x-x_1)-\frac{D^2}{R\cos^2\beta}\int_{-s_1}^{s}ds\int_{-s_1}^{s}hds. \quad (35)$$

The difference in position between the EFF and the SCOFF rays at the exit is clearly

$$\Delta y=D^2I_1/R\cos^2\beta, \quad (36)$$

where the integral I_1 is

$$I_1=\int_{-s_1}^{\infty}ds\int_{-s_1}^{s}(h_0-h)ds. \quad (37)$$

On the entrance side there is a similar displacement, given also by Eq. (36), but of course with the entrance angle α replacing the exit angle β.

The integral (37) is quite amenable to numerical solution. For the long-tail curve of Fig. 3, it has been determined as $I_1=0.491$ by the aid of a planimeter.

The results of the calculations of the particle motion in the median plane are that outside the magnet all EFF rays are parallel to the corresponding SCOFF rays. This means that there is no change in focal strengths in the median plane. At the exit, as well as at the entrance, a new center line is defined (EFF in Fig. 1). *All first-order coefficients of transfer pertaining to median-plane motion, including* (y/δ) *and* (y'/δ) *remain the same in the change from a SCOFF to an EFF case.*

Returning now to the z-direction motion, we make the simplifying assumption that the particle under consideration is moving parallel to the central ray with constant z inside the magnet; that is, $(dz/dx)_1=0$ and $(dy/dx)_1=s_1D/R\cos\beta$. We can then also put $z=$constant in Eq. (28), since any fractional change in z over the extent of the fringing field, where the integration is performed, will be of second order in D/R. This approach is equivalent to regarding the fringing field as a thin lens for z-direction focusing. It is clear from the outset that there will be no difference between z positions at the exit for the EFF and SCOFF cases. The slopes will be different, however. Integrating the leading terms in Eqs. (27) and (28) once, with the use of Eq. (15), we get

$$\frac{dy}{dx}=\frac{D}{R\cos\beta}\left(s_1-\int_{-s_1}^{s}hds\right)=\frac{D}{R\cos\beta}\int_{s}^{\infty}hds$$

and

$$dz/dx=-(z/R)\tan\beta(1-h).$$

These expressions are inserted into the higher-order terms of Eq. (28). After integration from $-s_1$ to infinity, we then have

$$\Delta\left(\frac{dz}{dx}\right)=\frac{z}{R}\tan\beta+\frac{zD}{R^2\cos\beta}\int_{-s_1}^{\infty}\frac{dh}{ds}\int_{s}^{\infty}hds$$
$$-\frac{zD^2\tan\beta}{R^3\cos^3\beta}\int_{-s_1}^{\infty}(h-h^2)ds\int_{-s_1}^{\infty}hds.$$

The last term is of second order in D/R, and we therefore neglect it. Using Eq. (8), we obtain

$$\frac{R}{f_z}=\tan\beta+\frac{D}{R\cos\beta}\int_{-s_1}^{\infty}\frac{dh}{ds}ds\int_{s}^{\infty}hds. \quad (38)$$

For the SCOFF case the second term is zero. The term therefore represents directly a correction for the EFF case of first order in D/R. We express this correction as

$$\Delta(R/f_z)=-I_2D/R\cos\beta, \quad (39)$$

where the integral I_2 is

$$I_2=-\int_{-s_1}^{\infty}\frac{dh}{ds}ds\int_{s}^{\infty}hds. \quad (40)$$

The correction for the entrance focal strength is found by replacing β with α in Eq. (39). These correction terms affect all four first-order z-direction transfer coefficients of Eqs. (3) and (4). Planimetric determinations of the integral (40) for the long-tail curve yields $I_2=0.487$.

Computer Work on Trajectories in Magnets with Straight Pole Boundaries

A computer program[7] has been written to determine the exact motion of charged particles in homogeneous field magnets with fringing field as given by Eqs. (13) and (20)–(22). Modifications of these equations have also been made so as to include the effects of curved pole boundaries as well as of the proximity of corners. The results of ray-

[7] The program in its original form was developed at M. I. T. by Miss Elizabeth Campbell, Lab for Nuclear Science Progress Report, 1 November 1961, p. 130.

tracing calculations, discussed in this section, pertain to magnets with straight pole boundaries and very wide pole pieces (no effects from nearby corners). In general, very good agreement is found between the computer results and the theory outlined above. In particular, the dependence of Δy and $\Delta(R/f_z)$ upon D and R indicated in Eqs. (36) and (39) is verified. When the machine-calculated y displacements and focal strengths R/f_z are compared with the predictions of Eqs. (36) and (39), it is found that the two integrals (37) and (40) for the long-tail curve should be $I_1=0.491$ and $I_2=0.475$. This is in very good agreement with the results from the planimeter integration mentioned above. For the short-tail field, the integrals are $I_1=0.309$ and $I_2=0.414$.

The results discussed in the following are all from calculations on the short-tail fringing field. However, there is not likely to be any principal difference between the short-tail and long-tail results.

The dependence of Δy [Eq. (36)] upon β or α has been verified, although a small modification, as explained below, is necessary to obtain high accuracy. The dependence of $\Delta(R/f_z)$ upon β or α is found to be stronger than Eq. (39) indicates. For these reasons, the results of the computer work are expressed in a somewhat different form, as follows:

$$\Delta y=(D^2/R)f_1(\beta_1) \tag{41}$$

and

$$R/f_z=\tan[\beta-(D/R)f_2(\beta_1)]. \tag{42}$$

The two functions $f_1(\beta_1)$ and $f_2(\beta_1)$ are plotted in Fig. 4 for the short-tail fringing field versus the "effective" angle

$$\beta_1=\beta-(1.2D/R)I_2. \tag{43}$$

Here I_2 is the integral (40), also identical with $f_2(0)$.

The angle β_1 is actually the angle between the normal to the pole boundary and the particle trajectory somewhere in the middle of the fringing field. It is not surprising that this average or "effective" angle should replace β which is the angle between the normal and the trajectory outside the fringing field. This replacement actually amounts to also including higher-order terms of D/R into the formulas.

For the long-tail fringing field it is expected that the angular dependence will be essentially the same as for the short-tail field. In lieu of accurate calculations for this case, it is suggested that the functions in Fig. 4 be multiplied with the factors

$$f_1(0)_{\text{long tail}}/f_1(0)_{\text{short tail}}=0.491/0.309=1.59,$$

and

$$f_2(0)_{\text{long tail}}/f_2(0)_{\text{short tail}}=0.475/0.414=1.15.$$

In Eq. (43), of course, I_2 should have the value (0.475) given above for the long-tail field.

Results of Computer Work on Magnets with Curved Pole Boundaries and Magnets with Finite Pole Widths

The pole boundaries at entrance and exit are sometimes curved, since this often improves the focusing properties of the magnet (second-order focusing). A finite pole width also has the effect of curving the iso-induction lines; that is, lines drawn through points of equal induction (see Fig. 5). In addition to changes in the second-order coefficients, which we are not concerned with here, the curvature of the iso-induction lines causes some changes in the first-order focusing properties and in the center line position. These changes are in general not wanted, mainly because they are difficult to evaluate. They can be minimized, however, by correct design. It is assumed that the design is laid out on the basis of calculations with a sharp cutoff fringing field. The angle β is then, of course, the angle between the center line of the beam (SCOFF C. L. in Fig. 5) and the normal to the *virtual field boundary* at O, the point of intersection with the center line. In Fig. 5(b), in particular, this angle is identical with the angle between the center line and the normal to the *pole boundary* only if the virtual field boundary at O is parallel to the pole boundary. This will be the case, approximately, if O is equidistant from the corners A and B. In short, the SCOFF center line passes through the symmetry point on the virtual field boundary, *not* through the midpoint C between A and B at the entrance to the mechanical gap (dotted line). The actual beam is further displaced by the relatively small amount Δy given by Eq. (41).

The reason why it is so important to center the beam correctly relative to the pole pieces should be clear from a brief study of Fig. 5. In Fig. 5(b), for instance, the angle between the dotted line and the normal to the iso-induction lines is smaller than β in the whole region outside the gap. The effective exit angle is therefore smaller than β if the beam emerges along this line. If, however, the beam moves along the EFF line, it moves partly in a region of "instantaneous" exit angle larger than β, and after it crosses the s axis in a region of "instantaneous" exit angle smaller than β, the average may therefore be close to β. With instantaneous exit angle, we here mean the angle between the final beam direction and the normal to an iso-induction line at the point where the particle is at the moment.

A series of computer calculations have been performed with geometries of the kind shown in Fig. 5. These calculations indicate that the effect of pole-piece curvature and of the proximity of the corners on first-order focusing and on beam position is negligible, except when D/R is large and when particularly high accuracy is called for. The small effects found can be summarized as follows:

(1) There is a small change in deflecting power of the fringing field. Assume that the mathematical description

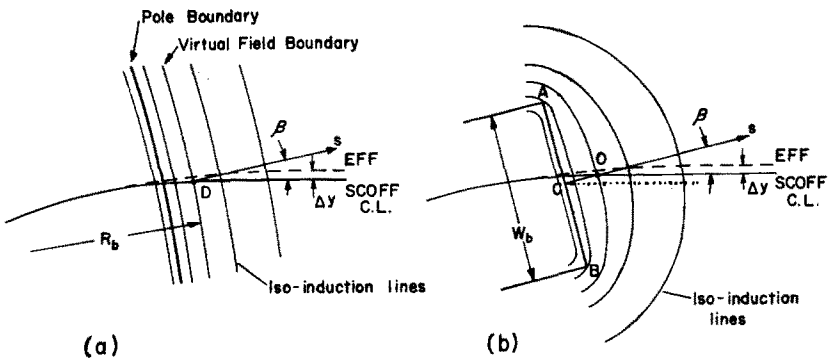

FIG. 5. Curvature of iso-induction lines caused by (a) curved pole boundaries, (b) proximity of pole corners.

of the fringing field is such that the net deflection is correct [Eq. (15) holds], when $\beta=0(\alpha=0)$. If $\beta\neq 0$, the rays get too little deflection in the fringing field when the iso-induction lines are curved. A semiempirical formula for this error is

$$\Delta y_c'=\left[\frac{D}{R_b}+1.4\frac{D^2}{W_b^2}\right]\frac{D}{R}f_3(\beta_1). \tag{44}$$

Here W_b is the width of the pole piece and R_b is the radius of curvature of the pole boundary [actually of the virtual field boundary, assuming $W_b=\infty$, see Fig. 5(a)]. The function $f_3(\beta_1)$ is plotted in Fig. 6. It is approximately proportional to $\tan^2\beta_1$.

The error $\Delta y_c'$ is quite small and can be corrected for in practice by a slight displacement of the pole boundary or by an increase in the field strength. In the computer work, it was convenient to have the central ray enter and exit in the right direction, and Eq. (44) was then used to estimate the necessary displacement of the pole boundaries. This displacement is

$$\Delta s_c=\Delta y_c' R\cos\beta/D.$$

(2) The curvature of the iso-induction lines, in effect, shortens the tail of the fringing field when $\beta\neq 0(\alpha=0)$. This results in a slight reduction of the displacement Δy of the center line. Examples: For $\beta=0.5$ rad, $R=30$ cm, and $D=5$ cm, the center line displacement is $\Delta y=3.18$ mm, when $R_b=\infty$ and $W_b=\infty$; it is 3.09 mm when $R_b=R$ and $W_b=\infty$; it is 3.03 mm when $R_b=R/2$ and $W_b=\infty$; finally, it is 3.09 mm when $R_b=\infty$ and $W_b=5D$. The reduction is thus quite small for reasonable values of the parameters.

(3) The effect of the extended but straight fringing field on z-direction focusing, discussed in detail in previous sections and summarized in Eq. (42), has no counterpart in median-plane focusing. The change from a sharp cutoff field to an extended fringing field results in a loss in total focusing power, a loss that is carried exclusively by the z-direction focusing. The curvature of the iso-induction lines, on the other hand, gives rise to a small change both in z-direction and median-plane focusing. In fact, the change in focusing strength in both directions can be expressed through an effective change in β(or α). A theoretical estimate of the apparent change in β resulting from the curvature of the iso-induction lines yields

$$\Delta\beta_c=\left[\left(\frac{D}{R_b}\right)^2-2c_6\left(\frac{D}{W_b}\right)^2\right]\tan\beta\int_0^1 s^2dh. \tag{45}$$

Here c_6 is a constant that is used in the computer program to describe the curvature of the iso-induction lines resulting from the "corner effect" (finite W_b). The value of the constant is approximately $c_6\approx 0.3$, and the integral in Eq. (45) is of the order of magnitude of unity. A semiempirical formula replacing Eq. (45) has been derived on the basis of computer results. It is

$$\Delta\beta_c=\left[\left(\frac{D}{R_b}\right)^2-0.6\left(\frac{D}{W_b}\right)^2\right]f_4(\beta_1). \tag{46}$$

The function $f_4(\beta_1)$ is plotted in Fig. 6.

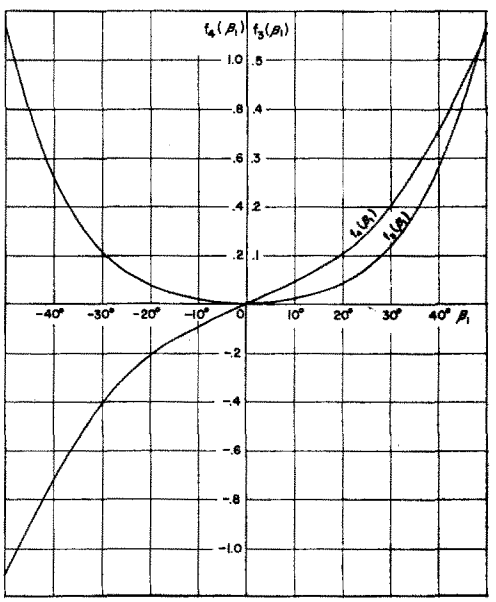

FIG. 6. Functions entering into Eq. (44) for loss of deflecting power caused by the curvature of the iso-induction lines and into Eq. (46) for the difference between "mechanical" and "magnetic" entrance or exit angle (based on the short-tail fringing-field curve).

V. CORRECTED FIRST-ORDER TRANSFER COEFFICIENTS

The preceding calculations are valid when (1) the magnet is designed so that the SCOFF center line crosses the virtual field boundary equidistant from the pole corners and (2) the actual beam center line (EFF in Fig. 5) is displaced from the SCOFF line by an amount Δy given by Eq. (41).

When these conditions are fulfilled, the first-order coefficients of transfer, given in Table I, can be used with the following modifications:

(1) In the six coefficients dealing with median-plane motion α and β should be replaced by

$$\alpha_M=\alpha+\Delta\alpha_c \tag{47}$$

and

$$\beta_M=\beta+\Delta\beta_c, \tag{48}$$

where $\Delta\beta_c$ is given by Eq. (46) and $\Delta\alpha_c$ can be found by substituting subscript a for subscript b and α for β in Eq. (46). The corrections $\Delta\alpha_c$ and $\Delta\beta_c$ are often so small that this modification may be neglected.

(2) In the four coefficients dealing with z-directional motion, α and β are replaced by [cf. Eq. (42)]

$$\alpha_Z=\alpha+\Delta\alpha_c-[D/R]f_2(\alpha_1) \tag{49}$$

and

$$\beta_Z=\beta+\Delta\beta_c-[D/R]f_2(\beta_1), \tag{50}$$

where β_1 and α_1 are given by Eq. (43).

If condition No. 1 above is not fulfilled, that is, if the beam is not correctly centered, the curvature of the isoinduction lines may result in angle corrections considerably larger than indicated by Eq. (46).

An Example

Consider a magnet with the following parameters: $R=27$ in., $\phi=45°$, $\alpha=2.2°$, $\beta=26.5°$, $D=2.5$ in., $R_a=R_b=\infty$, $W_a/D=W_b/D=5$.

From Eq. (41) and Fig. 4, we find the numerical value of the y displacement of the beam center line at the entrance $\Delta y_1=0.072$ in., and at the exit $\Delta y_2=0.087$ in.

By the aid of Eq. (46) and Fig. 6, we find that the corrections for the curvature effect are $\Delta\alpha_c=0°$ and $\Delta\beta_c=-0.4°$. For the first-order coefficients of transfer in the median plane, we therefore use $\alpha_M=2.2°$ and $\beta_M=26.1°$. The coefficients, calculated from the formulas of Table I, are given in the first two rows of Penner's[1] "horizontal" matrix

$$M_H=\begin{bmatrix} 0.736 & 0.707 & 0.293 \\ -0.319 & 1.053 & 0.851 \\ 0 & 0 & 1 \end{bmatrix}.$$

By the aid of Eqs. (49) and (50) and Fig. 5, we find that the effective entrance and exit angles for z-directional focusing are $\alpha_Z=0°$ and $\beta_Z=23.3°$. The coefficients for z-direction motion are given by the following, Penner's "vertical" matrix

$$M_V=\begin{pmatrix} 1 & 0.785 \\ -0.432 & 0.661 \end{pmatrix}.$$

A parallel beam incident on the magnet will be focused to a point in the median plane at a distance L_y from the exit, given by

$$\frac{L_y}{R}=-\frac{(y/y)}{(y'/y)}=\frac{0.736}{0.319}=2.31.$$

For the z-direction motion, focus will occur at L_z, given by

$$\frac{L_z}{R}=-\frac{(z/z)}{(z'/z)}=\frac{1}{0.432}=2.31.$$

The magnet thus gives a stigmatic image for an incident parallel beam at a distance $L=2.31R=62.4$ in. SCOFF calculations on the same magnet give $L_y=63.0$ in. and $L_z=50.0$ in. This illustrates very well the magnitudes of the effects discussed in this paper.

ACKNOWLEDGMENTS

I am very grateful to High Voltage Engineering Corporation for providing computer time and assistance for this work, to Mrs. Annija Galejs (HVEC) for her work on modifying the ray-tracing computer program and to Peter Hanley (HVEC) for operating it.